Design, Digital Control, and Simulation of a Grid-Connected Photovoltaic Generation System

Hazem Feshara*‡, Mohamed Elharony*, Soliman Sharaf*

*Department of Electrical Power and Machines, Faculty of Engineering, Helwan University, Egypt

(feshara@gmail.com, meeharony@yahoo.com, soliman-sharaf@hotmail.com)

‡ Corresponding Author; Hazem Feshara, 45 Borhan Street, Helwan, Cairo, Egypt, Tel: +20 100 176 1727, feshara@gmail.com

Received: 18.04.2014 Accepted: 12.05.2014

Abstract- This paper presents simulation and digital control of a three-phase grid-connected photovoltaic (PV) generation system. The technique used for maximum power point tracking (MPPT) of photovoltaic power is sliding mode (SM) control. Control of power extraction from DC link capacitor is presented. Space vector pulse width modulation (SVPWM) inverter is utilized to deliver power to utility grid. Simulation is performed using PLECS standalone software package and simulation results are shown. Complete theoretical foundation needed for system simulation is presented.

Keywords- Sliding mode control; solar energy; space vector pulse width modulation

1. Introduction

The need for power generation from renewable sources is rapidly increasing worldwide because they are more environment-friendly and because fossil fuels reserves are decreasing over time. Photovoltaic cells convert the free solar power to electric power. Power electronics and control techniques are the tools for the continuous research aiming to extract maximum power from PV cells at all conditions and convert such power to utilizable forms.

A photovoltaic (PV) cell converts light energy into electricity. Electrically connected PV cells form PV modules. PV modules are the fundamental building blocks of PV systems. To form a power generating unit, modules are arranged in an array and subjected to sunlight. Photovoltaic cell, module and array are illustrated in Fig. 1. PV power change frequently related to solar irradiation and cells temperature. At each condition, there is a voltage level at PV array terminals that gives maximum power. To extract that power, a widely used configuration is to connect the PV array to a DC-DC power converter. Sliding mode control (SMC) is a nonlinear control approach suitable for DC-DC converters achieving both robustness and stability [1]. Inverters convert DC voltage to AC voltage with required voltage and frequency. Modulation techniques are used to obtain variable output from inverters having a maximum fundamental component plus harmonics. Among these techniques, space vector pulse width modulation (SVPWM) is popular because it has various excellent features [2].

This paper describes simulation and control procedure for a grid-connected PV generation system. A PV array model was used in the simulation connected to a DC-DC converter controlled by a sliding mode controller. The capacitor at inverter output was used as the DC-link to the grid side inverter. A Controller for DC link voltage level and energy extraction was designed. Power, Voltage and current calculations and control were performed in dq synchronous frame. A phase locked loop (PLL) technique was implemented to synchronize the rotating frame with grid voltages. SVPWM technique synthesizes switching signals for inverter transistors given reference voltage and phase angle. The inverter is connected to the grid via an LC filter to reduce the harmonics caused by switching. Validity of proposed controllers is verified by simulation.

2. System Components

2.1. Photovoltaic Array Model

In this work, a PV module model with moderate complexity is used. Model circuit include a current source, a diode, and a series resistance R_S as shown in Fig. 2. The current source output I_L is directly proportional to the light G falling on cells and dependent on temperature T and voltage V. Model circuit and equations are described in [3]. The

calculated current characteristic of the PV module is implemented in PLECS using a 3-D lookup table [4]. Table outputs a 3-D function using interpolation or extrapolation.

A number of series connected modules form a string. Increasing the number of modules in a string increases the total output voltage. Strings are connected in parallel to increase the total power output and form a PV array. To model a string, the voltage input to the lookup table is formed by dividing the output voltage by the number of modules in the string as shown in Fig. 3. To model an array, the current output of the lookup table is multiplied by the number of strings in parallel.

2.2. DC-DC Power Converter

In order to adapt to the large variable range of the solar intensity, a buck-boost type DC-DC converter topology is used to transfer power from PV array as shown in Fig. 4 [5]. u represents the switch function of the power switch device. When u = 1, switch SW is close while u = 0, means SW is open. This configuration allows the control to switch abruptly between two system structures: 1) structure where the switch is open, 2) structure where the switch is closed.

The DC-link capacitor at DC-DC converter output is considered as the energy source for the inverter. The value of the DC-link capacitor C_{DC} is selected as follows [6]

$$C_{DC} = \frac{0.03\,X}{(1.8V_m)^2-(1.4V_m)^2} \quad (1)$$

Where, X is the system power rating and V_m is the system peak voltage

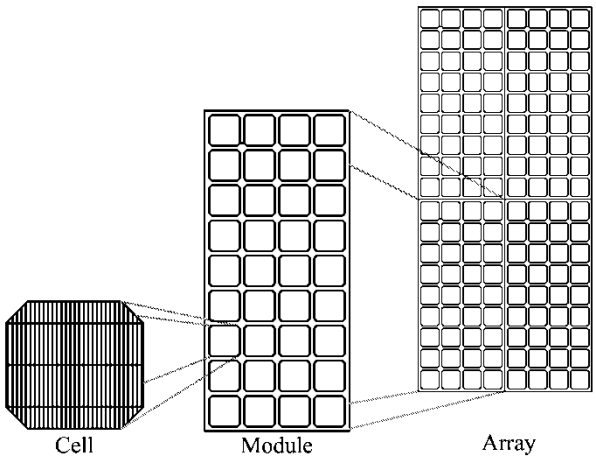

Fig. 1. Photovoltaic cell, module and array

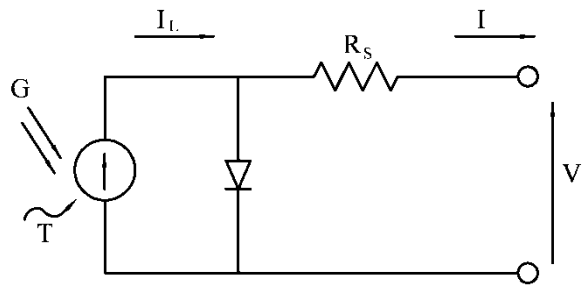

Fig. 2. Circuit diagram of the PV module model

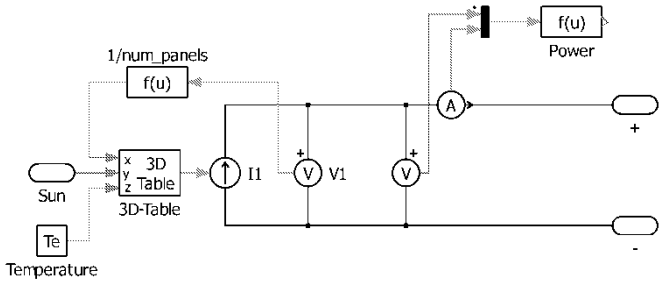

Fig. 3. PLECS implementation of PV module

2.3. Voltage Source Inverter

A three-phase Voltage Source Inverter (VSI) generates at each output phase i (i = a,b,c) a voltage V_i with two-level rectangular waveform. Phase switching sequence is controlled by modulation according to a given reference V_i*, so that the phase voltage low-order harmonics result in a voltage V_i (mean average) whose waveform should follow V_i* as close as possible. Modulation also generates high order harmonics around the switching frequency [7]. Fig. 5 shows PLECS circuit diagram of a VSI consisting of six Insulated Gate Bipolar Transistors (IGBT) having integrated anti-parallel diodes.

2.4. LC Filter

In order to reduce high order harmonics caused by switching, a low pass filter at inverter terminals is needed to fulfill power quality requirements.

A LC-filter is commonly used for that purpose [8]. Design procedure for the filter is explained as follows [9];

Calculate R_{base} for rated power P and nominal voltage V

$$R_{base} = \frac{V^2}{P} \quad (2)$$

$$f_c = \frac{1}{10} f_{sw} \quad (3)$$

$$LC = \left(\frac{1}{2\pi f_c}\right)^2 \quad (4)$$

Calculate L_f and C_f of the LC filter

$$L_f = \frac{R_{base}}{2\pi f_c \xi_c} \quad (5)$$

$$C_f = \frac{\xi_c}{2\pi f_c R_{base}} \quad (6)$$

Where, ξ_c is the filter damping factor. Fig. 6 shows circuit diagram of LC filter per phase. Where, R_f is the inductance branch resistance, R is the output branch resistance

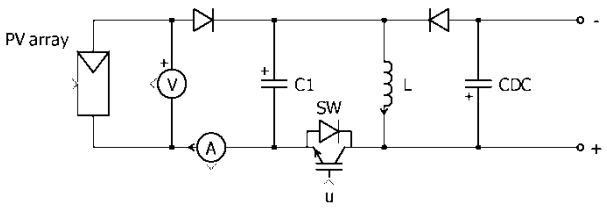

Fig. 4. PLECS circuit diagram of DC-DC converter

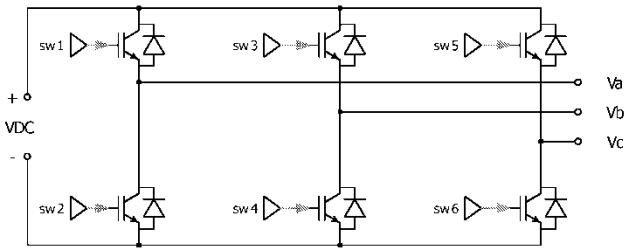

Fig. 5. PLECS circuit diagram of VSI

3. System Control

3.1. Photovoltaic Array Maximum Power Point Tracking

To achieve maximum power point tracking (MPPT), slide control method for the buck-boost converter is used. Sliding mode control (SMC) is well known for its robustness. Its most important feature is the invariance, giving independence of model uncertainties and strong disturbance rejection. SMC is a part of variable structure control that switches between system structures [10].

PV array power curve shown in Fig. 7 shows that $dP/dV > 0$ on the left of the maximum power point and $dP/dV < 0$ on the right. On that basis, converter switching function u is expressed as[5], [11]

$$u = \begin{cases} 1, & S < 0 \\ 0, & S \geq 0 \end{cases} \tag{7}$$

Where,

$$S = \frac{dP}{dV} = I + V\,\frac{dI}{dV} \tag{8}$$

The PLECS subsystem block shown in Fig. 8 was designed to calculate function u from PV voltage and current. To work in discrete-time, PV voltage and current are sampled at an interval T. A five point quadratic smoothing function is used for each signal to reduce noise in sampled data as described in [12]. Smoothing function could be written in the z-domain as

$$\frac{Y(z)}{U(z)} = \frac{31z^4 + 9z^3 - 3z^2 - 5z + 3}{35z^4} \tag{9}$$

Then, dI/dV is estimated using discrete transfer function for voltage and current as follows

$$\frac{I(z)}{F(z)} = \frac{z-1}{T\,z} \tag{10}$$

$$\frac{V(z)}{F(z)} = \frac{z-1}{T\,z} \tag{11}$$

$$\frac{\Delta I(z)}{\Delta V(z)} = \frac{I(z)}{F(z)} \Big/ \frac{V(z)}{F(z)} \tag{12}$$

After calculation of function S from equation (8), u is obtained from equation (7) using PLECS relay block.

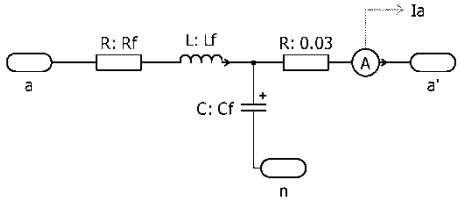

Fig. 6. PLECS circuit diagram of LC filter per phase a

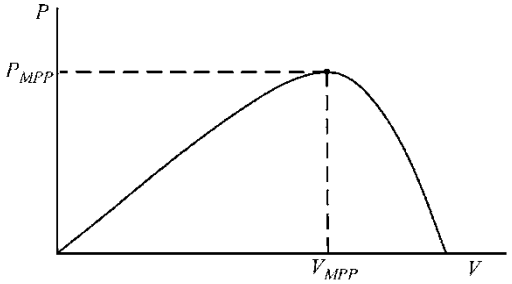

Fig. 7. PV array power curve

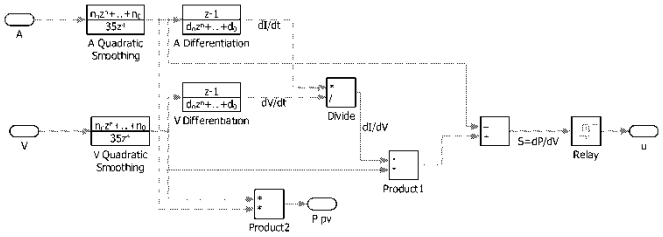

Fig. 8. PLECS subsystem block for estimation of function u

3.2. Energy Based DC Link Voltage Control

The DC-link capacitor at DC-DC converter output is considered as the energy source for the VSI. DC voltage V_{dcref} required at inverter input is calculated from phase-to-neutral grid voltage rms value V_{rms} as follows

$$V_{dcref} = \frac{3\sqrt{3}}{\pi}\,V_{peak} \tag{13}$$

Where,

$$V_{peak} = \sqrt{2}\,V_{rms} \tag{14}$$

The energy W_{DC} required from the DC-link capacitor C_{DC} to discharge from actual voltage V_{DC} to the reference value V_{dcref} is given as [6]

$$W_{DC} = \frac{1}{2}C_{DC}\left({V_{DC}}^2 - {V_{dcref}}^2\right) \tag{15}$$

Because the DC-link capacitor voltage has ripples with frequency double that of the supply frequency, The DC power P'_{DC} required from the capacitor is given as

$$P'_{DC} = \frac{W_{DC}}{T_c} \tag{16}$$

Where, T_c is the ripple period of the DC-link capacitor voltage and equals half the period of one AC cycle. Steady-state error is eliminated by adding an integral term. This controller is shown in Fig. 9 and the reference DC power P_{ref} is computed as

$$P_{ref} = K_{pe}\left({V_{DC}}^2 - {V_{dcref}}^2\right) + K_{ie}\int\left({V_{DC}}^2 - {V_{dcref}}^2\right)dt \tag{17}$$

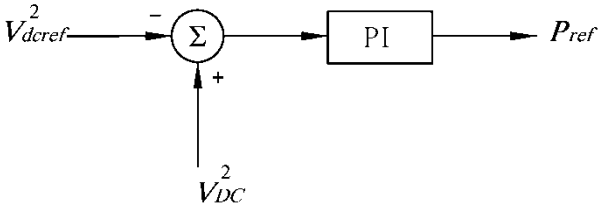

Fig. 9. DC-link voltage controller

Proportional and integral gains K_{pe} and K_{ie} of the controller could be given as [6]

$$K_{pe} = \frac{C_{DC}}{2T_c} \quad (18)$$

$$K_{ie} = \frac{K_{pe}}{2} \quad (19)$$

The discrete transfer function of integral is estimated as

$$\frac{Y(z)}{F(z)} = \frac{Tz+T}{2z-2} \quad (20)$$

3.3. Current Control of Voltage Source Inverter

The grid connected system aims to transfer maximum solar array energy into grid with a unity power factor. So, the system has to control active power *P* and reactive power *Q*. For that purpose, dq transformation of voltage and current are performed. The transformation matrix *K* is given as

$$K = \frac{2}{3}\begin{pmatrix} \cos\theta & \cos(\theta-120^0) & \cos(\theta+120^0) \\ \sin\theta & \sin(\theta-120^0) & \sin(\theta+120^0) \end{pmatrix} \quad (21)$$

Where, θ is the rotating dq frame angle. θ is synchronized with the phase angle of grid voltage giving *d* component of grid voltage equal to zero. *d* and *q* components of three phase voltages and currents are given as follows

$$\begin{pmatrix} V_d \\ V_q \end{pmatrix} = K \begin{pmatrix} V_a \\ V_b \\ V_c \end{pmatrix} \quad (22)$$

$$\begin{pmatrix} I_d \\ I_q \end{pmatrix} = K \begin{pmatrix} I_a \\ I_b \\ I_c \end{pmatrix} \quad (23)$$

To extract the phase angle of grid voltage, a PLL technique was implemented as shown in Fig. 10. Grid voltages $V_{a,b,c}$ are first transformed into dq components. Then, the PLL is locked by setting the reference *d* component voltage e_d* to zero. A PI controller is used to control V_d and bring it to zero. Grid nominal frequency is then added to the output of the controller. The resulting frequency is then integrated to give the grid locked angle θ [13]. PLECS math function *mod* is added at the output to bring the output back to zero after each time the value 2Π is reached.

The instantaneous power *S* delivered to the grid is given as [14], [15]

$$S = P + jQ \quad (24)$$

where

$$P = \frac{3}{2}\left(V_d I_d + V_q I_q\right) \quad (25)$$

$$Q = \frac{3}{2}\left(V_q I_d - V_d I_q\right) \quad (26)$$

In synchronous dq rotating frame, V_d=0. Therefore

$$P = \frac{3}{2}\left(V_q I_q\right) \quad (27)$$

$$Q = \frac{3}{2}\left(V_q I_d\right) \quad (28)$$

The active power *P* and reactive power *Q* are controlled by I_q current and I_d current respectively [15]. To transfer DC link power P_{ref} to the grid with zero reactive power we have the following reference currents

$$I_{qref} = \frac{2}{3}\frac{P_{ref}}{V_q} \quad (29)$$

$$I_{dref} = 0 \quad (30)$$

For a grid-connected inverter, the output voltages in the dq frame are given by [16]

$$\begin{pmatrix} U_d \\ U_q \end{pmatrix} = L\frac{d}{dt}\begin{pmatrix} I_d \\ I_q \end{pmatrix} + R\begin{pmatrix} I_d \\ I_q \end{pmatrix} + \omega L\begin{pmatrix} -I_q \\ I_d \end{pmatrix} + \begin{pmatrix} V_d \\ V_q \end{pmatrix} \quad (31)$$

To calculate reference voltage at inverter output, considering the *RL* circuit of the grid filter, we have

$$U_{dref} = \frac{d(I_{dref}-I_d)}{dt}L_f + (I_{dref}-I_d)R_f + V_d - \omega L_f I_q \quad (32)$$

$$U_{qref} = \frac{d(I_{qref}-I_q)}{dt}L_f + (I_{qref}-I_q)R_f + V_q + \omega L_f I_d \quad (33)$$

So, the differences between measured inverter output currents (I_d, I_q) and desired reference currents are input to PD controllers. Proportional and derivative gains for the controllers are R_f and L_f respectively. This actually means the required voltage at inverter output is higher than the grid voltage with the value that causes the required current to flow from the inverter to the grid through the filter with cross-coupling between the *d* and *q* components. The discrete Transfer function of derivative is estimated as

$$\frac{I(z)}{F(z)} = \frac{z-1}{T\,z} \quad (34)$$

Complete current control loop is shown in Fig. 11 [17], [18].

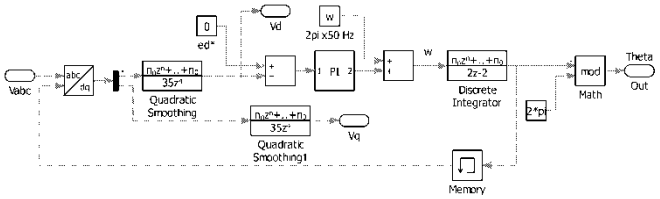

Fig. 10. PLECS subsystem block of a PLL system

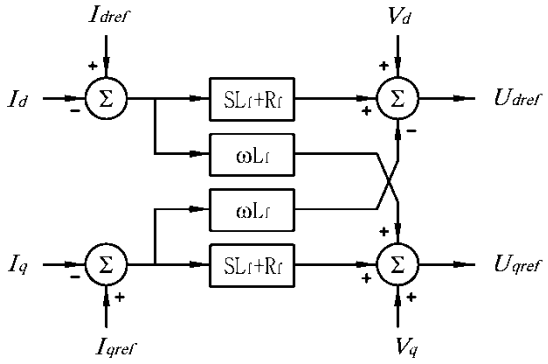

Fig. 11. Grid current control including cross-coupling terms

3.4. Space Vector Pulse Width Modulation

Space vector modulation (SVM) is a popular modulation technique for PWM inverter with various advantages. In SVM, there are eight possible unique states, each of which determines a voltage space vector. As shown in Fig. 12, six voltage space vectors shape the axis of a hexagon and divide the whole space into six sectors from 1 to 6. In addition, there are two zero vectors, U_0 and U_7 which lie at the origin. Therefore, SVM is a digital modulating technique with the objective of giving an appropriate combination of these eight vectors to approximate a given reference voltage. SVPWM is implemented as follows [13]:

3.4.1. Computation of reference voltage and angle

$\bar{U}_{ref}$ is the required reference voltage vector. Current control outputs were U_{dref} and U_{qref} as shown in Fig. 11. Magnitude U_{ref} and angle θ_{ref} of vector $\bar{U}_{ref}$ are obtained as follows: First, U_{dref} and U_{qref} are mapped to the complex orthogonal (αß) plane using the following transformation

$$\begin{pmatrix} U_\alpha \\ U_\beta \end{pmatrix} = \begin{pmatrix} \cos\theta & -\sin\theta \\ \sin\theta & \cos\theta \end{pmatrix} \begin{pmatrix} U_d \\ U_q \end{pmatrix} \quad (35)$$

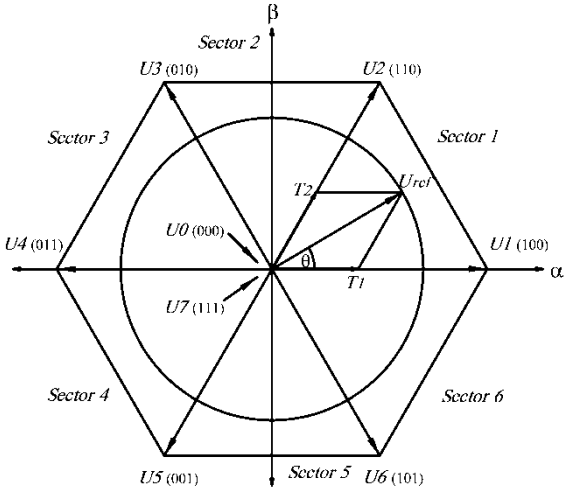

Fig. 12. Voltage Space Vectors in SVPWM

Where, θ is the angle between the rotating and stationary frame calculated by the PLL system. Next, U_{ref} and angle θ_{ref} are calculated as

$$U_{ref} = \sqrt{U_\alpha^2 + U_\beta^2} \quad (36)$$

$$\theta_{ref} = \tan^{-1}\frac{U_\beta}{U_\alpha} \quad (37)$$

3.4.2. Determination of sector number

Angle θ_{ref} is compared to angles range of sectors 1 to 6 so as to determine the sector in which θ_{ref} lies. A PLECS subsystem block is designed and used for sector determination as shown in Fig. 13. The angle θ_m in the range (0 – 60°) inside the sector is calculated as

$$\theta_m = \theta_{ref} - \frac{\pi}{3}(Sector - 1) \quad (38)$$

3.4.3. Determination of switching time intervals

The modulation index *m* is calculated as

$$m = \frac{U_{ref}}{V_{DC}/2} \quad (39)$$

The switching time intervals T_1, T_2, T_0 are calculated as

$$T_1 = \frac{\sqrt{3}}{2} T_{sw} m \sin\left(\frac{\pi}{3} - \theta_m\right) \quad (40)$$

$$T_2 = \frac{\sqrt{3}}{2} T_{sw} m \sin(\theta_m) \quad (41)$$

$$T_0 = T_{sw} - T_1 - T_2 \quad (42)$$

Where, T_{sw} is one switching interval for one leg of inverter transistors. $T_{sw} = 1 / f_{sw}$ (f_{sw} = Switching frequency)

3.4.4. Determination of switching pattern

Several solutions are available for synthesizing switching signals for inverter transistors. One solution is to start and end the switching interval with a zero vector. This solution is preferred because it reduces the number of switching events for the transistors. An example of such switching is shown in Fig. 14. A complete switching pattern lookup table for all switching signals at the 6 sectors is shown in Table 1 [2]. The lookup table is implemented in PLECS using three function blocks generating three ON intervals T_a, T_b, T_c of the three phases. Expressions of the three functions are shown in table 2.

Table 1. Switching Pattern Lookup Table

Sector	Upper Switches (*S1*, *S3*, *S5*)		
	S1	*S3*	*S5*
1	$T_1 + T_2 + T_0/2$	$T_2 + T_0/2$	$T_0/2$
2	$T_1 + T_0/2$	$T_1 + T_2 + T_0/2$	$T_0/2$
3	$T_0/2$	$T_1 + T_2 + T_0/2$	$T_2 + T_0/2$
4	$T_0/2$	$T_1 + T_0/2$	$T_1 + T_2 + T_0/2$
5	$T_2 + T_0/2$	$T_0/2$	$T_1 + T_2 + T_0/2$
6	$T_1 + T_2 + T_0/2$	$T_0/2$	$T_1 + T_0/2$

Table 2. Function Blocks Expressions

Interval	*Expression*
T_a	(u[4]==1)*(u[1]+u[2]+u[3])+(u[4]==2)*(u[1]+u[3])+(u[4]==3)*(u[3])+(u[4]==4)*(u[3])+(u[4]==5)*(u[2]+u[3])+(u[4]==6)*(u[1]+u[2]+u[3])
T_b	(u[4]==1)*(u[2]+u[3])+(u[4]==2)*(u[1]+u[2]+u[3])+(u[4]==3)*(u[1]+u[2]+u[3])+(u[4]==4)*(u[1]+u[3])+(u[4]==5)*(u[3])+(u[4]==6)*(u[3])
T_c	(u[4]==1)*(u[3])+(u[4]==2)*(u[3])+(u[4]==3)*(u[2]+u[3])+(u[4]==4)*(u[1]+u[2]+u[3])+(u[4]==5)*(u[1]+u[2]+u[3])+(u[4]==6)*(u[1]+u[3])

Where, $u[1] = T_1$, $u[2] = T_2$, $u[3] = T_0/2$, $u[4] = Sector$

3.4.5. Generating transistors switching signals

To start and end the switching interval with a zero vector, the repeating triangular wave shown in Fig. 15 is

used [19]. Switching signals are generated by comparing intervals T_a, T_b, T_c to the triangular wave as shown in Fig. 16.

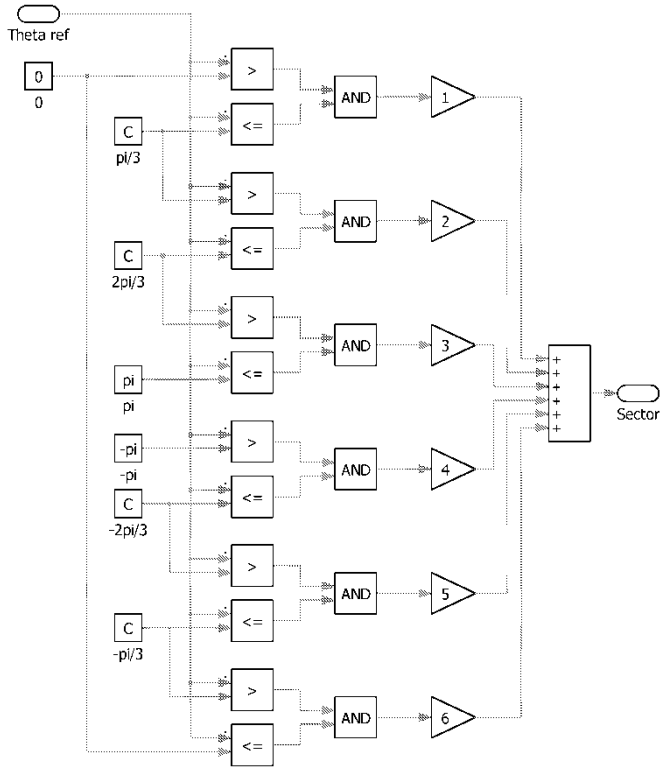

Fig. 13. PLECS subsystem block for sector identification

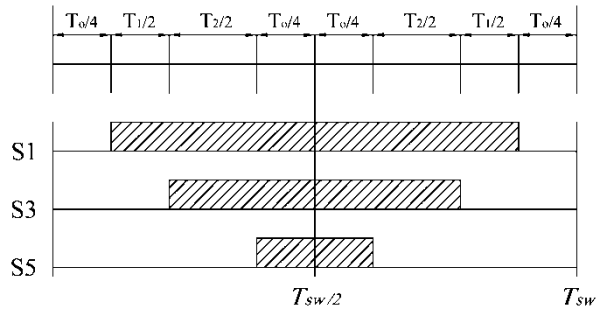

Fig. 14. Switching pulse pattern for three phases in sector 1

4. Simulation

4.1. Simulation Parameters

A 6 kilowatts system consisting of **BP365 65W** modules was simulated using PLECS software package to validate the proposed system design. Table 3 shows the parameters of simulation.

4.2. Simulation Results

Several situations of irradiance were input to the system at the PV modules input Sun (1 Sun = 1000Wm^{-2}). Grid voltages and currents in response to the irradiance situations are recorded and power delivered to the grid is calculated. Fig. 17 shows system response to irradiation step of 1 Sun followed by a step change to 0 Sun. Fig. 18 shows system response to irradiation input varying from 1 Sun to 0 Sun at a 4 Hz Frequency. Fig. 19 shows system response to irradiation input increasing and decreasing between five irradiation levels. Simulation shows increase of grid current and power in response to increase of irradiation with fast response except at system startup.

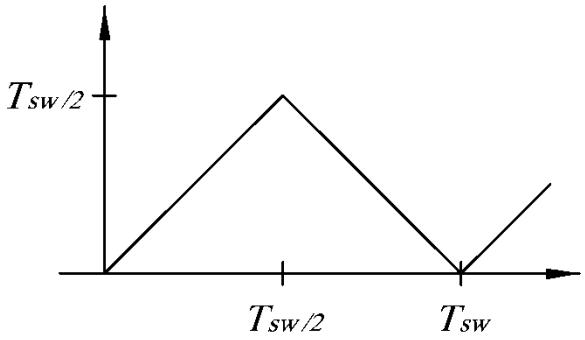

Fig. 15. Triangular wave parameters

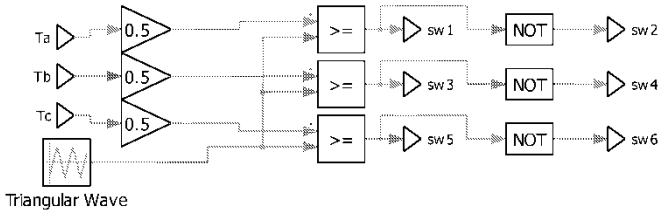

Fig. 16. Transistors switching signals generation

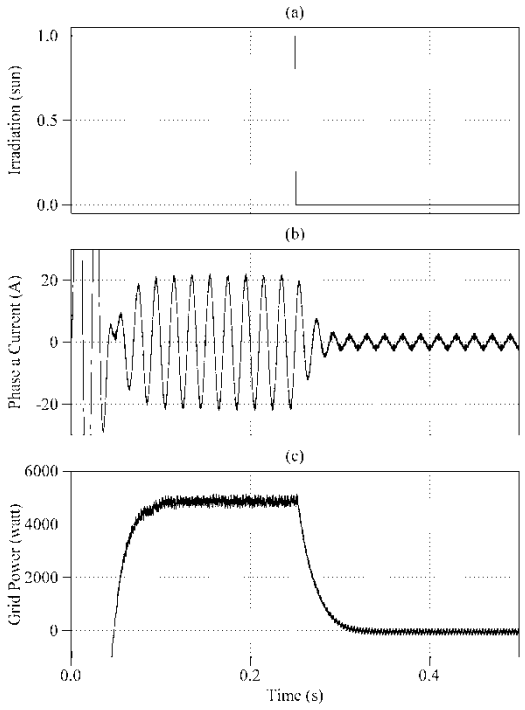

Fig. 17. Simulation Result of the PV Generation System: (a) Irradiation step input. (b) Current output at phase *a*. (c) Power output to grid.

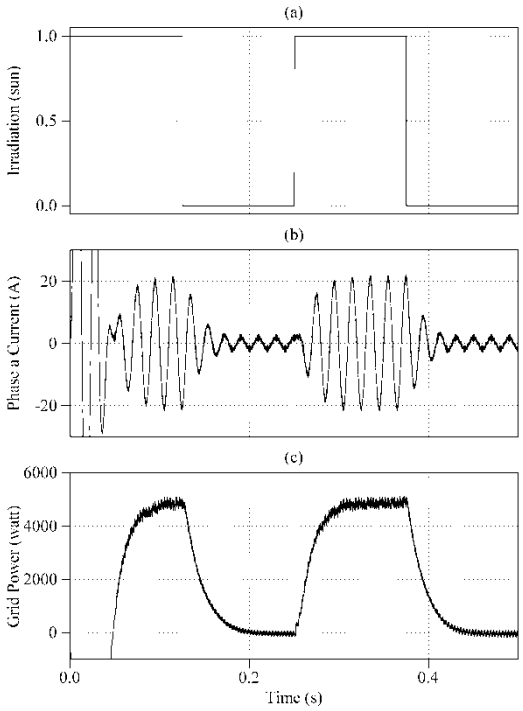

Fig. 18. Simulation Result of the PV Generation System: (a) Irradiation input varying between 1 and 0. (b) Current output at phase *a*. (c) Power output to grid.

Table 3. Simulation Parameters

	Parameter	***Description***	***Value***
	Num_panels	*Number of series connectd panels in the string*	*22*
	N_p	*Number of PV strings connected in parallel*	*4*
	C_1	*Output Capacitance connected across the PV strings*	*1000μF*
	T_e	*Operating temperature of the PV strings*	*25 ^{0}C*
	ω	*Angular frequency*	*2Π*50 rad/Sec*
	L	*DC-DC power converter Inductance*	*5mH*
	T	*Sampling interval*	*0.25mSec*
	V_{rms}	*Grid Voltage*	*110V*
0	$f_{sw} = 1/T_{sw}$	*Switching frequency*	*4kHz*
1	ξc	*Filter damping factor*	*0.5*
4	R_f	*Grid filter Resistance*	*1.2Ω*
5	T_c	*Ripple period of the DC-link capacitor*	*0.01Sec*

5. Conclusion

In this paper, a grid-connected PV generation system including a sliding mode MPPT technique was studied. A suitable LC grid filter was chosen, and grid current was controlled in dq synchronous frame by controlling the voltage output of VSI. The whole system was simulated and subjected to different solar irradiation inputs. Simulation results shows solar power converted to electric power and output to the grid. It is also seen that the amount of grid power is related to the input irradiation. Simulation shows that output currents and power takes time in the order of few tenths of a second to stabilize in following the input irradiation at system startup.

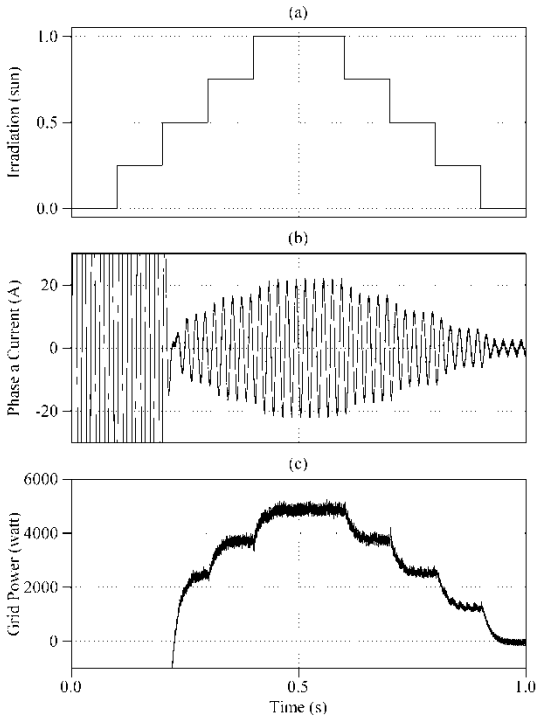

Fig. 19. Simulation Result of the PV Generation System: (a) Irradiation input varying between 5 levels. (b) Current output at phase *a*. (c) Power output to grid.

References

[1] H. Guldemir, "Modeling and sliding mode control of dc-dc buck-boost converter," in *Proc. 6th Int. advanced technological Symp*., May 2011, vol. 4 , pp. 475-480.

[2] D. Rathnakumar, J. LakshmanaPerumal, T. Srinivasan, "A new software implementation of space vector PWM," in *Proc. IEEE SoutheastCon*, 2005, pp.131-136.

[3] G. Walker, "Evaluating MPPT converter topologies using a MATLAB PV model", *J. Elect. Electron. Eng*., vol. 21, no. 1, pp. 49 -56, 2001.

[4] J. Schnberger. (2009, Sept.). *Modeling of a photovoltaic string using plecs*. [online]. Available: www.plexim.com.

[5] M. Zhang, J. Wu, H. Zhao, "The application of slide technology in PV maximum power point tracking system," in *Proc. 5th World Congr. Intell. Control and Automation*, 2004, vol. 6, pp. 5591-5594.

[6] K. K. Kora, "A fuzzy logic dc-Link voltage controller for three-phase DSTATCOM to compensate ac and dc loads," in *Proc. Int. J. of Scientific & Eng. Research*, 2011, vol. 2, Issue 10, pp. 190-202.

[7] L. Malesani, P. Tomasin, "PWM current control techniques of voltage source converters-a survey," in *Proc. Int. Conf. Ind. Electron. Control Instrumentation*, 1993, vol. 2, pp. 670-675.

[8] O. Mo, M. Hernes, K. Ljøkulsjøy, "Active damping of oscillations in LC-filter for line connected, current controlled, PWM voltage source converters," in *Proc. 10th European Conf. Power Electron. Applicat*., Toulouse, 2003.

[9] H. Kim , T. Yu, S. Choi, "Indirect current control algorithm for utility interactive inverters in distributed generation systems," *IEEE Trans. Power Electron*., vol. 23, no. 3, pp.1342 -1347, May 2008.

[10] J. Dannehl, F. W. Fuchs "Discrete sliding mode current control of three-phase grid-connected PWM converter," in *Proc. 13th European Conf. Power Electron. Applicat., 2009* , pp. 1-10.

[11] T. Esram, P. L. Chapman, "Comparison of Photovoltaic Array Maximum Power Point Tracking Techniques," *IEEE Trans. Energy Conv*., vol. 22, no. 2, pp.439-449, 2007.

[12] P. A. Gorry, "General least-squares smoothing and differentiation by the convolution (Savitzky-Golay) method." *Analytical Chemistry*, vol. 62, no. 6, pp. 570-573, 1990.

[13] A. Abdalrahman, A. Zekry, A. Alshazly, "Simulation and implementation of grid-connected inverters," *Int. J. Computer Applicat*., vol. 60, no. 4, pp. 41-49, December 2012.

[14] R. Teodorescu, M. Liserre, and P. Rodriguez, *Grid converters for photovoltaic and wind power systems*, IEEE/Wiley, 2011.

[15] I. S. Kim, "Robust maximum power point tracker using sliding mode controller for the three-phase grid-connected photovoltaic system," *Solar Energy*, vol. 81, issue 3, pp. 405 -414, March 2007.

[16] Y. Yong, R. Yi, S. Huan-qing, T. Yan-yan, Y. Ying, "Grid-connected inverter for wind power generation system," J. Shanghai University (English Ed.), vol. 13, issue 1, pp. 51-56, February 2009.

[17] M. Milosevic, "Decoupling control of d and q current components in three-phase voltage source inverter," ETH Zurich, Tech. Rep., 2003.

[18] Y. Sozer, D. A. Torrey, "Modeling and Control of Utility Interactive Inverters," *IEEE Trans. Power Electron.*, vol. 24, no.11, pp. 2475-2483, Nov. 2009.

[19] E. Hendawi, F. Khater, A. Shaltout, "Analysis, simulation and implementation of space vector pulse width modulation inverter", in *Proc. 9th Int. Conf. on Applicat. Elect. Eng*., 2010, pp. 124-131